Thin Solid Films 517 (2009) 5773–5778

Contents lists available at ScienceDirect

Thin Solid Films

journal homepage: www.elsevier.com/locate/tsf

Precise etch-depth control of microlens-integrated intracavity contacted vertical-cavity surface-emitting lasers by in-situ laser reflectometry and reflectivity modeling

Y.M. Song [a], K.S. Chang [b], B.H. Na [a], J.S. Yu [c], Y.T. Lee [a,*]

[a] Department of Information and Communications, Gwangju Institute of Science and Technology, 1 Oryong-dong, Buk-gu, Gwangju 500-712, Republic of Korea
[b] Division of Instrument Development, Korea Basic Science Institute, 113 Gwahangno, Yusung-gu, Daejeon, 305-333, Republic of Korea
[c] Department of Electronic Engineering, Kyung Hee University, 1 Seochon-dong, Gihung-gu, Youngin-si, Gyeonni-do 446-701, Republic of Korea

ARTICLE INFO

Article history:
Received 20 July 2008
Received in revised form 25 March 2009
Accepted 25 March 2009
Available online 2 April 2009

Keywords:
Etching
Multilayers
Optoelectronics devices
Semiconductor

ABSTRACT

We studied the etch-depth control of 980 nm intracavity contacted vertical-cavity surface-emitting laser (VCSEL) structures with GaAs/AlGaAs distributed Bragg reflectors by in-situ laser reflectometry and reflectivity modeling in $SiCl_4$/Ar inductively coupled plasmas. Highly accurate etch-depth control can be achieved by counting the number of oscillation peaks in the experimental reflectance signal through the fitting of the reflectivity data calculated theoretically using a transfer matrix method. The fits provide a very good agreement, allowing us to distinguish individual layers precisely and stop the etching at a desired depth. After confirmation of the validity of in-situ dry etch monitoring, this technique was employed in the fabrication of microlens-integrated intracavity contacted VCSELs including composition-graded digital alloy AlGaAs for high precision control of the etch depth in intracavity region. The etch-depth difference between calculated and experimental results was kept below 20 nm, indicating a good etch performance. The spatial uniformity of ~5% was obtained over 1×1 cm^2 sample size.

1. Introduction

Vertical-cavity surface-emitting lasers (VCSELs) have attracted great interest as a standard light source for many applications including optical communications, short-haul data links, and optical computing because it has advantages of low cost, low power consumption, high speed modulation, and surface-normal emission [1]. For these applications, high data rate and low heat dissipation in VCSELs are essential, requiring a low device resistance. Recently, intracavity contacted VCSELs, consisting of undoped DBR mirrors and ring contacts on a semi-insulating substrate, have exhibited an improved performance over the conventional extracavity structures [2–4]. The use of intracavity contacts allows a current path by the p-type and n-type layers on either side of the active region. This leads to the decrease of series resistance and makes the contacts essentially coplanar, which are advantageous for high speed operation due to the reduced parasitic capacitance [5]. In addition, the asymmetric contact layout reduces an unfavorable current crowding effect at the oxide aperture region [6].

Furthermore, the monolithic integration of VCSELs with a semiconductor microlens without additional process steps showed the improvement of coupling efficiency to optical fibers or components [7,8]. In contrast to the extracavity structure, however, the operational characteristics of intercavity contacted VCSELs are very sensitive to the etch depth control exactly to the right position for p-contact and n-contact layers. Ohmic contacts cannot be formed if the layers are underetched while the significant overetch can cause an increase in the series resistance. Thus, the etch depth must be controlled in a precisely layer-by-layer manner during the etching process. In this structure, where no etch stop layer can be used, it may be difficult to accurately end the etching because the etch rate may vary to some extent from run to run for the same etching condition. To overcome these limitations, efficient etch monitoring technique is required. The laser reflectometry has been used for precise in-situ etch monitoring of thick multi-thin layer structures (eg., DBR stacks) [9–12]. However, there are only few reports on the in-situ etching of a full VCSEL structure having active layer and DBR mirrors.

In this paper, the etch–depth control with high precision during $SiCl_4$/Ar inductively coupled plasma (ICP) etching of microlens-integrated intracavity contacted VCSEL structures with thick multi-thin layers was investigated by in-situ laser reflectometry, together with reflectivity modeling.

2. Experiment and reflectivity modeling

Fig. 1 shows the schematic diagram of the 980 nm microlens-integrated intracavity contacted VCSEL structure used in this experiment. All layers were grown on semi-insulating GaAs substrates by a molecular beam epitaxy (DCA P600). The active region consists of three 8.5 nm-thick u-$In_{0.19}Ga_{0.81}As$ wells with 10 nm-thick u-GaAs barriers, sandwiched by 106.1 nm u-$Al_{0.32}Ga_{0.68}As$ cladding layers to

* Corresponding author. Tel.: +82 62 970 2206; fax: +82 62 970 3128.
E-mail address: ytlee@gist.ac.kr (Y.T. Lee).

0040-6090/$ – see front matter © 2009 Elsevier B.V. All rights reserved.
doi:10.1016/j.tsf.2009.03.198

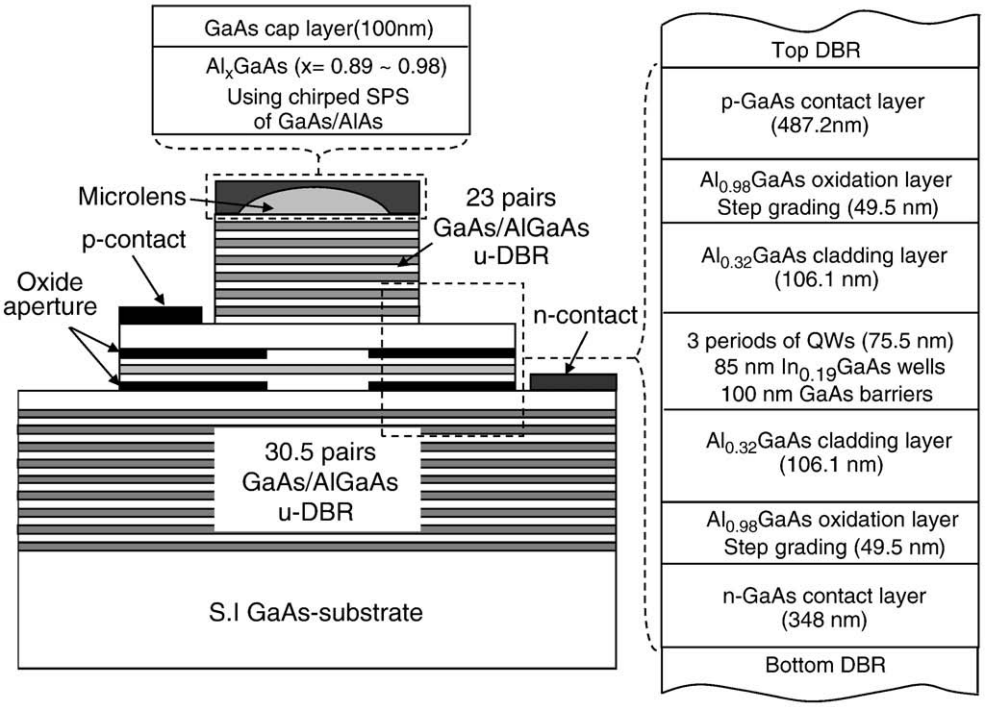

Fig. 1. Schematic diagram of the 980 nm microlens-integrated intra-cavity contacted VCSEL structure used in this experiment.

form a 1λ-thick cavity and 49.5 nm-thick p/n-$Al_{0.98}Ga_{0.02}As$ oxidation layers. It is surrounded by $7\lambda/4n$-thick p- and $5\lambda/4n$-thick n-GaAs contact layers. The bottom and top DBR mirrors consists of 30.5 and 22 pairs of λ/4-thick u-GaAs/$Al_{0.88}Ga_{0.12}As$ layers, respectively. The thickness of p- and n-contact layers should be carefully selected considering top and bottom DBR mirrors, respectively, given by $d = (2\ k + 1)\lambda/4n_{ref}$, where d is the thickness of contact layer, $k = 0$, 1, 2, …, λ is the operation wavelength, n_{ref} is the refractive index of layer [13]. The 1.3 μm-thick composition-graded digital alloy $Al_xGa_{1-x}As$ ($x = 0.89$–0.98) was formed on the top DBR mirror. The chirped short-period superlattices (SPS) of AlAs (16–90 ML)/GaAs (2 ML) in 75 steps was used to grade the composition of the AlGaAs. Using a selective oxidation process, this technique enables the formation of self-aligned microlens. The structure was completed by a 100 nm thick GaAs cap layer.

The Etch experiments were carried out by using an ICP etcher (Oxford Instruments Plasmalab System 100). In order to achieve anisotropic, low damage, and nonselective etching for GaAs/AlGaAs

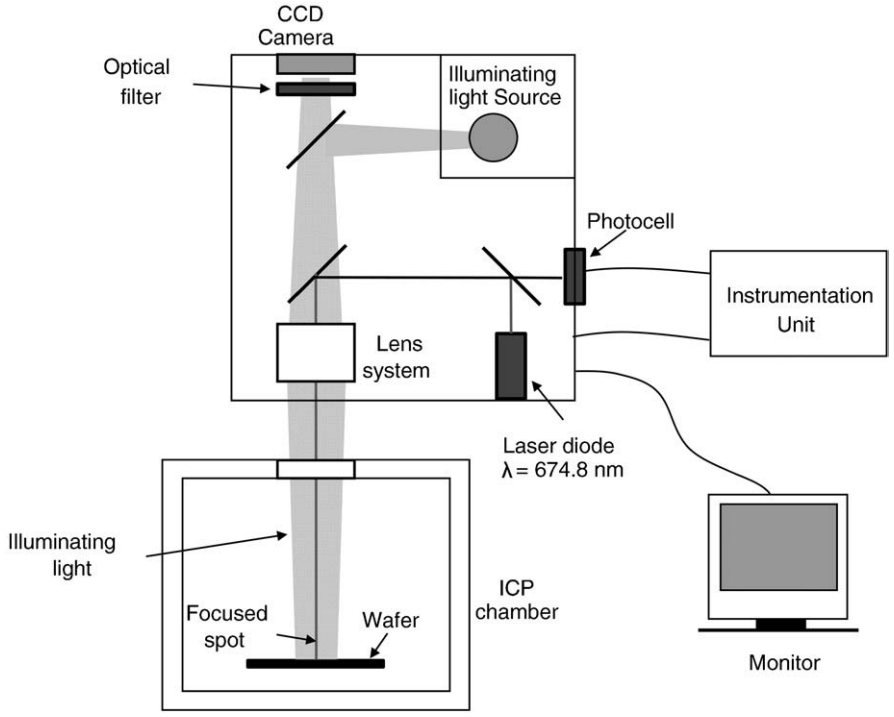

Fig. 2. Experimental set-up of in-situ dry etch monitoring using a laser interferometer system (Jobin–Yvon Horiba, DIGILEMS).

structures, the $SiCl_4$/Ar mixture gas was used. For the generation of plasma, 13.56 MHz radio frequency (rf) power is applied to both ICP source and substrate electrode. The ion energy at the substrate, which is controlled mainly by the rf power supplied to the electrode, is monitored by the dc bias measured in real time. Samples on 2 in. silicon carrier wafer were loaded into the vacuum chamber through a load lock. To provide a good thermal conductivity between the wafer and chuck, helium pressure was applied to the back of the wafer. The samples were etched at an optimum condition, i.e., $SiCl_4$ (7.5 sccm)/Ar (25 sccm) with rf power of 50 W and ICP power of 200 W under a gas pressure of ~0.27 Pa.

The experimental set-up of in-situ dry etch monitoring using a laser interferometer system (Jobin-Yvon Horiba, DIGILEMS) is shown in Fig. 2. The spot of laser beam ($\lambda = 674.8$ nm) is focused on the surface of the sample by adjusting its spot position, and then the reflected signal is detected by a silicon photocell [14]. The signal is processed by the instrumentation unit connected to a personal computer for monitoring. Etch depths of all samples were measured using a surface profiler. Additionally, the scanning electron microscopy (SEM, Hitachi, S-4700) measurements were performed at an operating voltage of 15 kV to measure an accurate etch depth and to investigate the etched profile. The atomic force microscopy (AFM, XE-200, Park Systems) measurements are also carried out using Si cantilever (NCHR, Nanosensor) on the etched sample in the non-contact mode.

To find the depth at which it is desired to stop the etching process, the experimental reflectance signal containing oscillations was compared to the theoretical curve calculated by reflectivity modeling. Using a transfer matrix technique, the reflectivity of remaining part of the structure was calculated. The etch process is simulated by removing the top layer successively, leading to a resultant reflectivity, and then this process was repeated until the substrate is exposed.

3. Results and discussion

To investigate the validity of in-situ etch monitoring during the etching process, the initial experiments towards controlling the etch depth of the intracavity contacted VCSEL structure (including intracavity region and DBR mirrors) and the composition-graded digital alloy AlGaAs structure for microlens were carried out separately. Fig. 3 shows (a) the calculated reflectivity as a function of etch depth and (b) the reflectance intensity measured experimentally during etching in $SiCl_4$/Ar as a function of etch time for the intracavity contacted VCSEL structure. The reflectivity signals were observed distinctly in three different regions, namely, top DBR (22 pairs), intracavity/contact layers, and bottom DBR (30.5 pairs), creating beat patterns accompanying the oscillations. For the top DBR, the upper and lower peaks of reflectivity signal correspond to the GaAs layer of 69.6 nm and the $Al_{0.88}Ga_{0.02}As$ layer of 80.5 nm, respectively, thus producing the 22 beat patterns of the peak to peak. In this calculation, the refractive indices of 3.784-*j*0.164 and 3.141 were used for the GaAs and $Al_{0.88}Ga_{0.02}As$ layers, respectively [15,16]. This is also applied for the bottom DBR which consists of 30.5 pairs of GaAs/$Al_{0.88}Ga_{0.02}As$ in the same way.

As shown in Fig. 3(b), the experimentally measured reflectance signal is in good agreement with the calculated reflectivity signal except 0 positions. The offset between simulation and measurement is a result of the time required for removing the native oxide on the sample surface at the start of the etch process to reach the underlying semiconductor layers [9,10]. The delay time is not constant and it depends on the thickness of the native oxide by exposure to atmosphere (oxygen). In this case, the resulting delay time of ~18 s was observed. The total etch time and etch depth are about 910 s and 9.2 μm, respectively, for this VCSEL structure, indicating an average etch rate is 10.1 nm/s. While the etch rate in top GaAs/$Al_{0.88}Ga_{0.02}As$ DBR was ~9.9 nm/s, the etch rate increased slightly to ~10.5 nm/s for

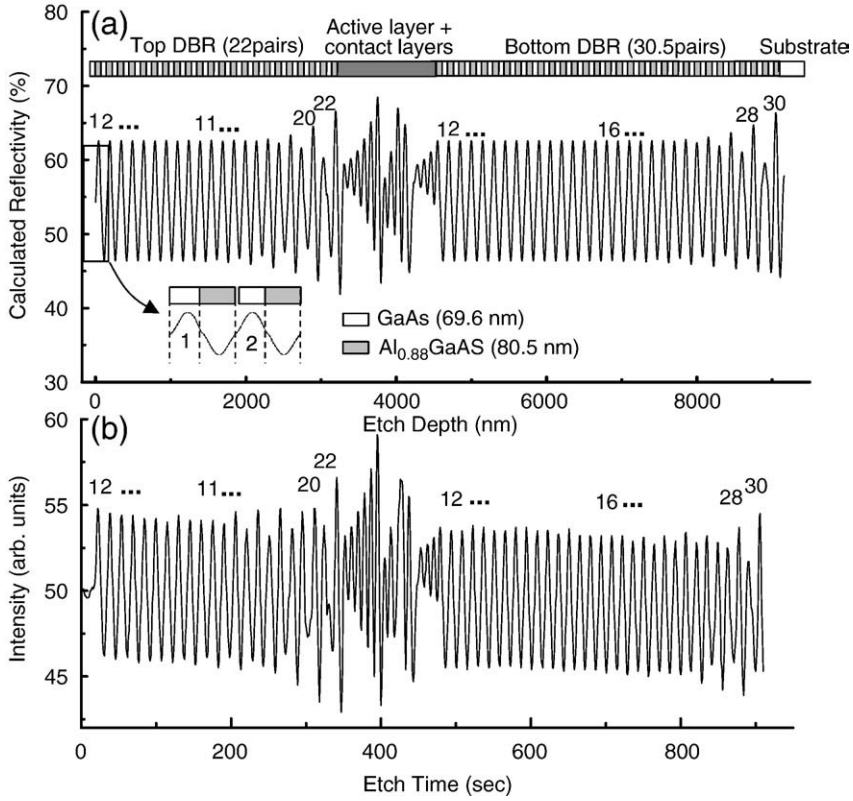

Fig. 3. (a) Calculated reflectivity as a function of etch depth and (b) the reflectance intensity measured experimentally during etching in $SiCl_4$/Ar as a function of etch time for the intracavity contacted VCSEL structure.

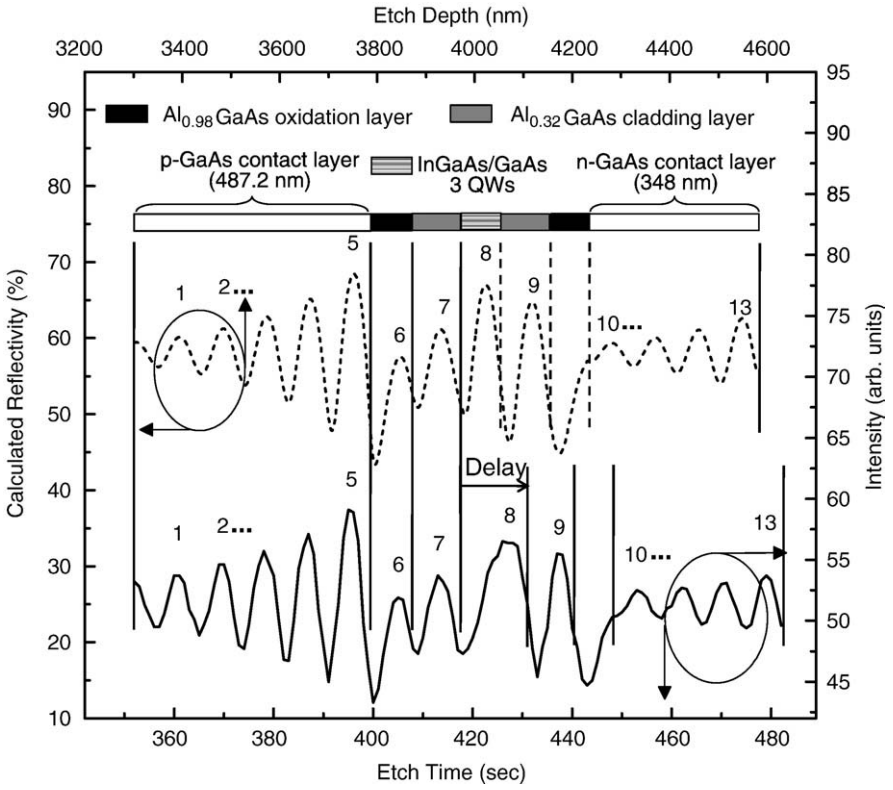

Fig. 4. Calculated reflectivity and reflectance intensity measured experimentally for the magnified portion of intracavity/contact layers.

the bottom DBR, i.e. by 6%. Without in-situ etch monitoring, therefore, it is difficult to control an etch target depth accurately and repeatably because of the unpredictable time delay by the surface oxide and the gradual change in etch rate [12]. It is noted that the large signal to noise ratio was observed in Fig. 3 due to the large refractive index difference between the GaAs and $Al_{0.88}Ga_{0.02}As$ layers.

Fig. 4 shows the calculated reflectivity and the reflectance intensity measured experimentally for the magnified portion of intracavity/

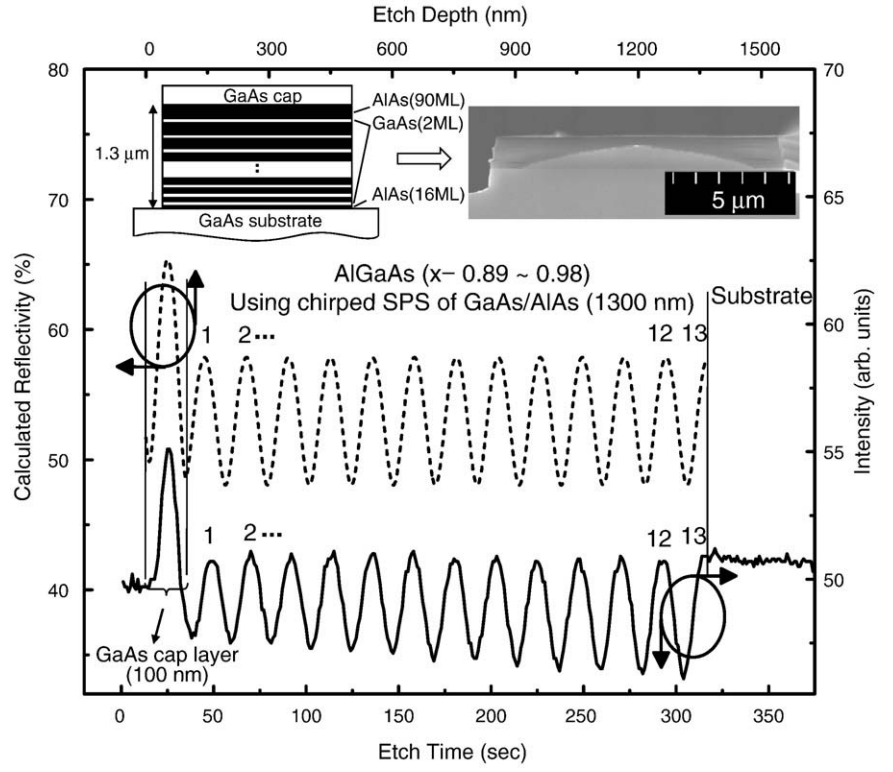

Fig. 5. Calculated reflectivity and reflectance intensity measured experimentally of the composition-graded digital alloy AlGaAs structure for microlens-integrated VCSELs.

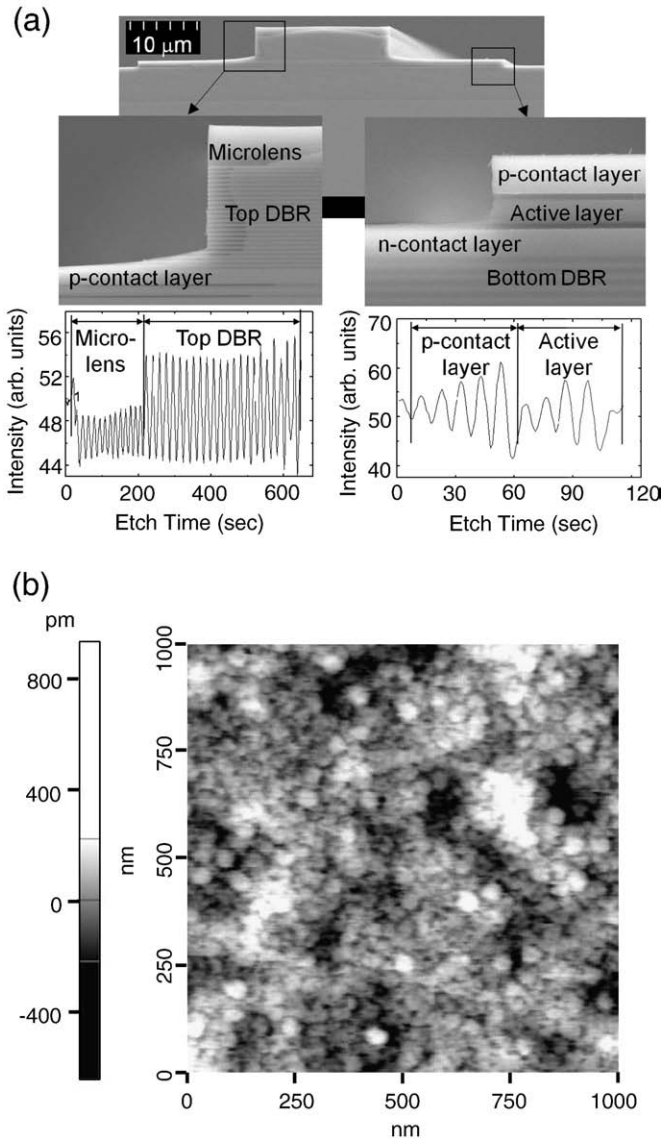

Fig. 6. (a) SEM images of the etched profiles of the microlens-integrated intracavity contacted VCSEL structure with selective oxidation and their reflectance intensities observed during the etching, and (b) AFM scan image on the surface of n-GaAs contact layer after the etching of intracavity layers.

contact layers. The intracavity region includes three periods of InGaAs/GaAs QWs, $Al_{0.98}Ga_{0.22}As$ oxidation layer, and $Al_{0.32}Ga_{0.68}As$ cladding layer. In the intracavity/contact regions, the reflectivity signal exhibits somewhat complicated oscillations due to the multi-thin layers and the etch rate of 9.8 nm/s, on average, was observed. For the 487.2 nm-thick p-GaAs contact layer, the 5 beat patterns were observed after the etching and the peak to peak span corresponds to $\lambda/2n$ (i.e., 89.2 nm). The etch rate of 10.3 nm/s was obtained from the peak positions. Similarly, the 348 nm-thick n-GaAs contact layer corresponds to the 4 beat patterns, leading to an etch rate of 10.2 nm/s. From this result, it is found that the etch selectivity of $Al_xGa_{1-x}As$ over GaAs is ~1:1 in $SiCl_4$/Ar plasma because the average etch rate of 10.1 nm/s was obtained for GaAs/$Al_{0.88}Ga_{0.02}As$ DBRs. For the inter-cavity region, the peak to peak span changes from 109.4 nm to 87.9 nm. There is a discrepancy between the calculated and experimental results after the $In_{0.19}Ga_{0.81}As$/GaAs QWs (8th layer) was etched. Thus, this delay is ascribed to the lower etch rate of InGaAs layer because the etch rate in numerical reflectivity model is assumed to be kept constant across the whole structure. Clearly, the etch rate was lowered to ~6.1 nm/s for the 8th layer including three $In_{0.19}Ga_{0.81}As$ wells. This means that the estimation of etch time from the peak to peak span is not frequently enough to guarantee the correct etch depth for the multi-thin layer structure. However, the accurate stop point control of the etching is possible by counting the number of oscillations in the experimental reflectance signal. In order to etch right up to the n-GaAs contact layer in the intracavity contacted VCSEL structure, the etching should be stopped exactly after counting the 9th peak, inferred from the reflectivity modeling as shown in Fig. 4.

Fig. 5 shows the calculated reflectivity and the reflectance intensity measured experimentally of the composition-graded digital alloy AlGaAs structure for microlens-integrated VCSELs. To form the self-aligned microlens on the VCSEL structure using selective oxidation [17], a 1.3 μm-thick chirped SPS of AlAs (16–90 ML)/GaAs (2 ML) in 75 steps were grown, as illustrated in the inset of Fig. 5. The chirped SPS layers are graded into digital alloy $Al_xGa_{1-x}As$ layers, where the Al composition (x) is linearly varied from 0.89 to 0.98. The SEM image shows the cross sectional view of chirped SPS mesa structure after the selective oxidation. However, it is difficult to resolve the composition-graded digital alloy AlGaAs layers in reflectivity modeling because the thickness of each layer is much thinner than the operating wavelength of incident light. In this case, the whole layer behaves as an optically homogeneous layer, so we used an average Al composition of $x=0.935$ and its refractive index for the reflectivity modeling. The observed reflectance signal after the etching is well consistent with the results calculated from the theoretical model used here, exhibiting 13 beat patterns.

Using both the in-situ laser reflectometry and reflectivity modeling, the $SiCl_4$/Ar ICP etching in two steps (i.e., 20 μm wide mesa for p contacts and 54 μm wide mesa for n contacts) was carried out for the fabrication of microlens-integrated intracavity contacted VCSELs. Fig. 6(a) shows the SEM images of the etched profiles of the microlens-integrated intracavity contacted VCSEL structure with selective oxidation and their reflectance intensities observed during the etching. For the p-contact mesa etching, the device structure was etched from the GaAs cap layer right up to the p-GaAs contact layer (by stopping the etching after counting the 36th peak) through the composition-graded digital alloy AlGaAs and top DBR. For the n-contact mesa etching, the p-GaAs contact layer and intracavity layers were etched right up to n-GaAs contact layer (by stopping the etching after counting the 9th peak). The magnified SEM images confirm a good control of etch depth with high resolution. The etch depths of p-contact mesa and n-contact mesa was measured using an SEM to be 3.32 μm and 942 nm, respectively. The measured etch depth is almost consistent with that expected, with an error of below 20 nm. The contact metals are formed on the slightly overetched surfaces (i.e., less tolerance than 4%) for 487.2 nm p- and 348 nm n-contact layers, which results in good device performance [8]. The spatial uniformity of 5% was observed across the sample of 1×1 cm^2 size. The AFM scan image on the surface of n-GaAs contact layer after the etching of intracavity layers is shown in Fig. 6(b). The root mean square (RMS) roughness of 0.15 nm for a scan area of 1×1 μm^2 was obtained, indicating a good morphology of etched surface.

4. Conclusions

The etch–depth control of intracavity contacted VCSEL structures was investigated by in-situ laser reflectometry using a $SiCl_4$/Ar ICP etching. The theoretical reflectivity curve gave a good agreement with the real-time reflection signal obtained from the laser reflectometry. The layer-by-layer in-situ etching in DBR mirror and active layer structures was achieved by counting the number of oscillation peaks in the laser reflection signal together with the fit of reflectivity modeling, making it possible to stop the etching at the desired depth. For the self-aligned microlens, the chirped SPS of AlAs/GaAs was modeled into composition-graded digital alloy $Al_xGa_{1-x}As$ layers with an average Al composition and its refractive index. This etching

technique was applied to the mesa etching for the p and n contacts of microlens-integrated intracavity contacted VCSELs. From the SEM image, the experimental etched profiles exhibited a slight overetch with a tolerance of less than 20 nm, indicating excellent etch performance. Also, the spatial uniformity of ~5% during the etching was observed over 1×1 cm^2 sample size. These results allow the possibility of an accurate control of etch depth with good surface morphology for the fabrication of microlens-integrated intracavity contacted VCSELs to achieve the high device performance.

Acknowledgement

This work was supported in part by the IT R&D program of MKE/IITA [2008-F-045-02] and by the GIST Top Brand Project (Photonics 2020).

References

[1] K. Iga, IEEE J. Sel. Top. Quantum Electron. 6 (2000) 1201.
[2] J.W. Scott, B.J. Thibeault, D.B. Young, L.A. Coldren, F.H. Peters, IEEE Photonics Technol. Lett. 6 (1994) 678.
[3] M.H. MacDougal, J. Geske, C.K. Lin, A.E. Bond, P.D. Dapkus, IEEE Photonics Technol. Lett. 10 (1998) 9.
[4] V.V. Lysak, K.S. Chang, Y.T. L ee, J. Optoelectron. Adv. Mater. 8 (2006) 355.
[5] G. Dang, W.S. Hobson, L.M.F. Chirovsky, J. Lopata, M. Tayahi, S.N.G. Chu, F. Ren, S.J. Pearton, IEEE Photonics Technol. Lett. 13 (2001) 924.
[6] A.V. Krishnamoorthy, L.M.F. Chirovsky, W.S. Hobson, J. Lopata, J. Shah, R. Rozier, J.E. Cunningham, L.A. D Asaro, IEEE Photonics Technol. Lett. 12 (2000) 609.
[7] S.H. Park, Y. Park, H. Kim, H. Jeon, S.M. Hwang, J.K. Lee, s.H. Nam, B.C. Koh, J.Y. Sohn, D.S. Kim, Appl. Phys. Lett. 80 (2002) 183.
[8] K.S. Chang, Y.M. Song, Y.T. Lee, IEEE Photonics Technol. Lett. 18 (2006) 2203.
[9] S.E. Hicks, W. Parkes, J.A.H. Wilkinson, C.D.W. Wilkinson, J. Vac. Sci. Technol. B 12 (1994) 3306.
[10] H. Moussa, R. Daneau, C. Meriadec, L. Manin, I. Sagnes, R. Raj, J. Vac. Sci. Technol. A 20 (2002) 748.
[11] H.K. Cho, J.Y. Lee, B. Lee, J.H. Baek, W.S. Han, J. Vac, Sci. Technol. B 17 (1999) 2626.
[12] S.N.M. Mestanza, N.C. Frateschi, J. Vac. Sci. Technol. B 19 (2001) 192.
[13] C. Wilmsen, H. Temkin, L.A. Coldren, Vertical-cavity surface-emitting lasers: Design, fabrication, characterization, and applications, Cambridge University Press, Cambridge, England, 1999.
[14] A. Holland, General training manual for Jobin-Yvon Horiba thin film group end point detection equipment, Jobin Yvon Ltd, 1999.
[15] S. Zollner, J. Appl. Phys. 90 (2001) 515.
[16] S. Gehrsitz, F.K. Reinhart, C. Gourgon, N. Herres, A. Vonlanthen, H. Sigg, J. Appl. Phys. 87 (2000) 7825.
[17] K.S. Chang, Y.M. Song, Y.T. Lee, IEEE Photonics Technol. Lett. 18 (2006) 121.